Photon Emission and Reabsorption Processes in $CH_3NH_3PbBr_3$ Single Crystals Revealed by Time-Resolved Two-Photon-Excitation Photoluminescence Microscopy

Takumi Yamada,[1] Yasuhiro Yamada,[2] Yumi Nakaike,[1] Atsushi Wakamiya,[1] and Yoshihiko Kanemitsu[1,*]

[1]*Institute for Chemical Research, Kyoto University, Uji, Kyoto 611-0011, Japan*
[2]*Department of Physics, Chiba University, Inage-ku, Chiba 263-8522, Japan*

The dynamical processes of radiative recombination of photocarriers and reabsorption of emitted photons in $CH_3NH_3PbBr_3$ single crystals are studied using time-resolved two-photon-excitation photoluminescence (PL) microscopy. We find that the PL spectrum and its decay dynamics depend on the excitation-depth profile. As the excitation depth increases, the PL spectrum becomes asymmetric, the peak energy redshifts, and the PL decay time becomes longer. These observations can be well explained by a simple model including photon recycling (photon emission and reabsorption) in thick samples with strong band-to-band transitions and high radiative recombination efficiencies.

I. INTRODUCTION

Outstanding progress has been made in lead halide perovskite $CH_3NH_3PbX_3$ (X = I, Br, Cl) solar cells since the first report in 2009 [1]. Thin-film solar cells based on perovskite $CH_3NH_3PbI_3$ have shown a rapid increase in conversion efficiency, now exceeding 22% [2]. Furthermore, lead halide perovskite semiconductors exhibit remarkable properties as thin-film solar-cell materials, such as large absorption coefficients, low nonradiative recombination rates, and long carrier diffusion lengths [3–8]. Since their absorption coefficients are comparable to those of GaAs, the incident photons are efficiently absorbed and converted to free photocarriers. Moreover, the observed high open-circuit voltage (approximately 1 V) in perovskite solar cells suggests small losses due to nonradiative carrier recombination or trapping of photocarriers [9]. The nonexcitonic and long-lived free-carrier dynamics of perovskites enable a long diffusion of photocarriers, which leads to high-power-conversion efficiencies in solar cells [10–12]. In order to achieve further improvements in solar-cell efficiency, a thorough understanding of the fundamental properties of lead halide perovskite materials is needed.

So far, extensive experimental studies have been carried out using thin-film samples, which usually exhibit a grain structure (typically several hundreds of nanometers in size). It is known that optical absorption and photoluminescence (PL) spectra depend on the grain structure of the thin film [13]. More specifically, it is considered that extrinsic defects and traps are formed mainly at grain boundaries rather than inside the grain [14]. The polycrystalline grain structure affects the diffusion and recombination processes of photocarriers in thin films. In fact, the PL dynamics of single crystals are different from those of polycrystalline thin films consisting of grains [11]. Two-photon-excitation spectroscopy on single crystals revealed that the PL decay dynamics in the near-surface region under one-photon excitation are different from those in the interior bulk region under two-photon excitation [11,12]. These observations were explained by photon recycling in thick $CH_3NH_3PbX_3$ (X = I, Br) perovskite single crystals [11,12], similar to the case of GaAs single crystals. In thick and highly luminescent semiconductors such as GaAs, long lifetimes are usually observed as a result of photon recycling or reabsorption of emitted photons by strong band-to-band transitions [15–17]. Because the evaluated PL efficiencies of $CH_3NH_3PbX_3$ perovskites are extremely high [18,19], photon recycling is important for this material class [11,12,18]. Very recently, Pazos-Outón *et al.* [18] also demonstrated that the photon recycling can enhance the carrier diffusion length and device performance of perovskite solar cells based on fitting the results of the spatially resolved PL and photocurrent (PC) profiles. In addition, Staub *et al.* [20] recently evaluated the effect of photon recycling on the radiative lifetime in perovskite thin films. In the photon-recycling process, reabsorption of the bulk PL efficiently generates additional carriers. Note that in this case, the measured PL lifetimes and carrier diffusion lengths are longer than the intrinsic lifetimes and diffusion lengths of semiconductors, which improves the solar-cell efficiency [21,22]. Therefore, the optical responses of thick $CH_3NH_3PbX_3$ are complicated, and even in single crystals, the photocarrier dynamics still remain unclear. The experimental verification of the change in PL lifetime under various excitation conditions is important for acquiring a deep understanding of photon emission and reabsorption processes, which is essential for practical device applications such as solar cells and light-emitting diodes.

[*]Corresponding author.
kanemitu@scl.kyoto-u.ac.jp

In this work, we study space- and time-resolved PL spectra of $CH_3NH_3PbBr_3$ single crystals by means of time-resolved two-photon-excitation PL microscopy. Because under two-photon excitation, the carrier density is proportional to the square of the excitation intensity, the photocarriers are selectively excited at the focal point, where the excitation intensity is high. By changing the focal point of the excitation laser, we clarify the influence of reabsorption on the PL from the interior region. As the distance between the focal point and surface increases, the PL peak redshifts, and the PL lifetime becomes longer. This behavior is explained by considering carrier diffusion and photon recycling. We clarify that the enhancement of the PL lifetime is caused by an intrinsic bulk property. The impact of photon recycling on the PL lifetime and carrier diffusion in $CH_3NH_3PbBr_3$ single crystals is discussed.

II. SAMPLES AND EXPERIMENTAL SETUP

$CH_3NH_3PbBr_3$ single crystals are fabricated by inverse-temperature crystallization [23]. The single crystals are prepared from a 1.0-M N, N-dimethylformamide (DMF) solution at 110 °C. Purified lead bromide (734 mg, 2.0 mmol) and methylammonium bromide (224 mg, 2.0 mmol) are dissolved in dry DMF (2.0 mL) at 70 °C by stirring. The resulting solution is poured into a screw-cap vial, which is placed on a hot plate at 110 °C for 2 d to produce a single crystal with dimensions of around $6 \times 5 \times 2$ mm³. The obtained single crystals are washed with dry hexane before being used for the measurements.

Time-resolved PL measurements are conducted using a monochromator and a streak camera; the time resolution is 50 ps. A femtosecond wavelength-tunable laser system sets to a repetition rate of 200 kHz and a pulse width of 250 fs is used for excitation. The excitation wavelength is 1028 nm, and the excitation fluence is 120 μW. Under this excitation condition, we consider that the photocarrier density is high enough that the bimolecular recombination dominates the recombination dynamics. The microscope setup allows us to probe at various depths by adjusting the focal position. A 100× objective lens is used to focus the excitation light and collect the fluorescence. The excitation and fluorescence light are separated by a short-pass filter. The size of the excitation spot is measured using a beam profiler. The excitation spot size at the beam waist is 4.1 μm, and the Rayleigh length of the excitation light is 23 μm. The sample is mounted on an xyz microstage for accurate positioning. The PL image is monitored using a complementary metal-oxide-semiconductor camera, and we define the zero point of the excitation depth to when the focal point falls on the surface of the sample. The excitation depth d is evaluated by using a micrometer scale to measure the distance change of the objective lens from the surface d_{shift} and considering the refractive index via

$$d = n_{ex}d_{shift}, \qquad (1)$$

where n_{ex} represents the material's refractive index for the excitation light ($n_{ex} = 1.97$) [24]. By checking the reproducibility of the PL spectrum, intensity, and dynamics before and after the experiments, we confirm that there is no effect due to sustained illumination of excitation light. This is contrary to the long-time dependence observed in thin films [25]. All experiments are conducted in vacuum at room temperature.

III. RESULTS AND DISCUSSION

Time-resolved PL measurements are conducted using two-photon-excitation microscopy with different excitation-depth profiles. The photocarriers are directly excited in the interior region, which suppresses the extrinsic effects such as surface oxidation and surface recombination. Figure 1(a) shows the PL spectra for different focal distances (in the following referred to as the excitation depth d, i.e., the distance of the excitation focal point from the surface) just after excitation (delay time: $t = 0$ ns). When the laser pulses are focused on the near-surface region ($d = 9.87$ μm), the PL peak appears at around 2.28 eV, and the spectral shape is symmetric. As d increases, a redshift in the PL peak energy is observed. In addition, the high-energy side of the PL spectrum shows a significantly lower intensity, and the shape of the PL spectrum becomes asymmetric. Such an excitation-depth dependence of the PL spectrum can be explained in terms of the reabsorption of luminescence from the interior region.
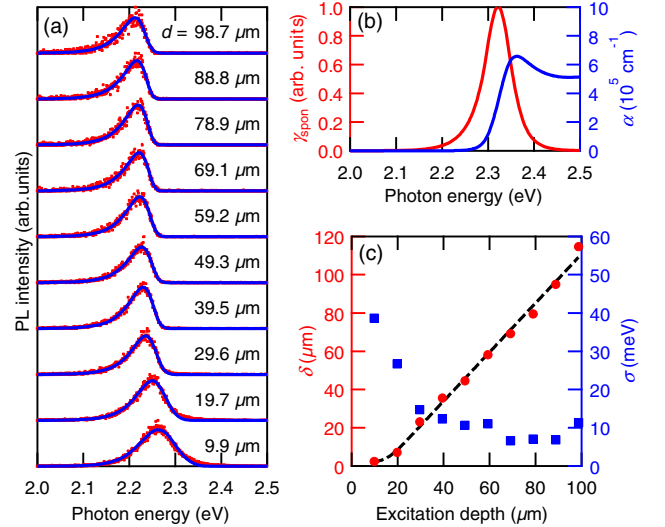
FIG. 1. (a) PL spectra at different focal distances (i.e., the distance of the excitation focal point from the surface, d) just after excitation (delay time: $t = 0$ ns). The solid blue lines are the fitting curves from Eq. (5). (b) Calculated spontaneous emission spectrum and absorption data from Ref. [24]. (c) Summary of fitting parameters (δ, red circle; σ, blue square). The dashed line is the fitting of δ by Eq. (7).

Lead halide perovskite semiconductors exhibit strong band-to-band transitions, large absorption coefficients, and small luminescence Stokes shifts [3,6,26]. Thus, photons emitted by radiative band-to-band recombination should be reabsorbed while traveling from the interior region towards the surface. Photons emitted by carrier recombination in deep regions of the sample are unable to reach the sample surface. In particular, photons with energies above the band-gap energy are strongly absorbed in the material. According to the Lambert-Beer law, the transmitted light intensity from the excitation spot towards the surface can be described as follows:

$$T(E, d) = e^{-\alpha(E)d}, \tag{2}$$

where $\alpha(E)$ and E represent the absorption coefficient and the photon energy, respectively.

In the single-crystal samples, the light emission is caused by spontaneous recombination. According to the van Roosbroeck–Shockley relation, the spontaneous emission spectrum $\gamma_{\mathrm{spon}}(E)$ at room temperature can be described as follows [27]:

$$\gamma_{\mathrm{spon}}(E) \propto n(E)^2 E^2 \alpha(E) \exp\left(-\frac{E}{k_B T}\right), \tag{3}$$

where $n(E)$, k_B, and T represent the refractive index, Boltzmann constant, and temperature, respectively. The observed PL spectrum is modified by intrinsic or extrinsic effects, such as thermal broadening and inhomogeneous broadening. The PL spectrum is also modified by the photon-reabsorption effect. To take the broadening and photon-reabsorption effects into account, the PL spectrum should be calculated with

$$I_{\mathrm{PL}}(E) \propto \iint\limits_{0}^{\infty} \gamma_{\mathrm{spon}}(\varepsilon)\rho(z)^2 T(\varepsilon, z) e^{-[(E-\varepsilon)/\sigma]^2} \frac{dz d\varepsilon}{\sqrt{\pi\sigma^2}}. \tag{4}$$

Here, z, $\rho(z)$, σ, and ε are the distance from the sample surface, the carrier depth profile, the Gaussian width of the total broadening, and the photon energy, respectively. We consider that the electron and hole densities are proportional to $\rho(z)$. For simplicity, we can approximate the carrier depth profile to a Dirac δ function as $\rho(z) \sim \delta_{\mathrm{func}}(z - \delta)$ because the carrier depth profile is quite sharp relative to the crystal thickness. Here, we introduce a mean depth δ, which represents the carrier distribution. Then, Eq. (4) can be simplified as follows:

$$I_{\mathrm{PL}}(E) \propto \int\limits_{0}^{\infty} \gamma_{\mathrm{spon}}(\varepsilon) T(\varepsilon, \delta) e^{-[(E-\varepsilon)/\sigma]^2} \frac{d\varepsilon}{\sqrt{\pi\sigma^2}}. \tag{5}$$

The PL spectra shown in Fig. 1(a) are numerically fitted using Eq. (5). The fitting parameters are the amplitude, δ, and σ. The absorption and refractive index data of a single

crystal in Ref. [24] are used for fitting. At the low-energy side (i.e., less than 2.29 eV), we estimate a band-tail absorption with an Urbach energy of 15 meV [26]. The absorption data and calculated spontaneous emission spectrum [see Eq. (3)] are plotted in Fig. 1(b). The peak energy of the spontaneous emission is located around 2.32 eV. This value is consistent with the one-photon excitation PL spectra of $CH_3NH_3PbBr_3$ single crystals reported previously [12] and is larger than all observed peak energies of the PL spectra in Fig. 1(a). In $CH_3NH_3PbBr_3$ single crystals, the luminescence below the band edge, which originates from shallow traps and defects, is enhanced in a similar manner as in thick III-V semiconductors [21,28,29].

The best-fit parameters are summarized in Fig. 1(c). The mean depth δ varies linearly with the excitation depth. The Gaussian width σ increases for shallower excitation near the sample surface. This is a result of a broader PL spectrum for shallower excitation, where the photons with energy higher than the band edge can also escape from the sample.

For a deeper understanding of the influence of reabsorption, we derive the relation between the mean depth δ and the excitation depth d. First, we approximate the carrier depth profile by a Gaussian function,

$$\rho(z) = \frac{1}{\sqrt{\pi w^2}} \exp\left[-\left(\frac{z - d}{w}\right)^2\right]. \tag{6}$$

Here, w is the Gaussian width of the depth profile. Then, the mean depth δ can be described as follows:

$$\delta(d) = \frac{\int_0^\infty z\rho(z)dz}{\int_0^\infty \rho(z)dz} = d + \frac{w \exp[-(\frac{d}{w})^2]}{\sqrt{\pi}\mathrm{erfc}(-\frac{d}{w})}, \tag{7}$$

where $\mathrm{erfc}(z)$ is the complementary error function. When fitting the data, we replace d with $a(d-d_0)$ in order to obtain a better fitting result. The fitting results obtained using Eq. (7) are also plotted as a dashed curve in Fig. 1(c). The best-fit parameters are $a = 1.3$, $d_0 = 14$ μm, and $w = 5.9$ μm. The fitting result of the data is almost linear. Therefore, the carrier density profile assumed in Eq. (6) is valid.

Furthermore, the spatial carrier redistribution can be discussed by analyzing the time dependence of the PL spectral shape. Figures 2(a) and 2(c) show the time evolution of the PL spectra for the cases of near-surface excitation ($d = 9.9$ μm) and deep excitation ($d = 98.7$ μm). The PL spectrum and dynamics depend on the excitation-depth profile. For the case of near-surface excitation ($d = 9.9$ μm), the PL peak just after excitation ($t = 0$ ns) is observed at 2.28 eV, and this peak redshifts with time. Additionally, the spectral shape changes from symmetric to asymmetric. The transient carrier distribution can be evaluated by fitting the PL spectral shape for different delay times. The fitting results for the case of surface excitation with different delay times are summarized in Fig. 2(b). According
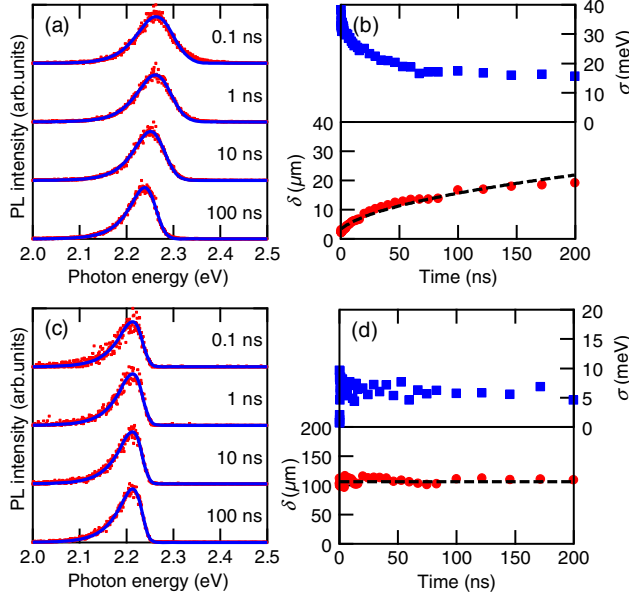
FIG. 2. (a) Time evolution of PL spectra for the case of near-surface excitation ($d = 9.9$ μm). (b) Fitting results of the PL spectra with different delay times for near-surface excitation. The dashed curve is the fitting result from Eq. (9). (c) Time evolution of PL spectra for the case of deep excitation ($d = 98.7$ μm). (d) Fitting results of the PL spectra with different delay times for deep excitation.

to this figure, the mean depth δ increases, and the Gaussian width σ decreases with time. These results suggest that the excited carriers diffuse from the sample surface towards the interior region.

Now we evaluate the expected time evolution of the mean depth induced by carrier diffusion. Considering that isotropic three-dimensional (hemispherical) carrier diffusion occurs from the sample surface towards the interior region, the Gaussian width of the depth profile can be described with

$$w(t) = \sqrt{w_0^2 + 4Dt}, \qquad (8)$$

where w_0, D, and t are the Gaussian width of the depth profile just after excitation, the diffusion constant, and the delay time, respectively. In case of surface excitation (substituting d with 0), Eq. (7) results in

$$\delta(t) = \frac{w(t)}{\sqrt{\pi}} = \sqrt{\frac{w_0^2 + 4Dt}{\pi}}. \qquad (9)$$

The time evolution of δ is fitted by Eq. (9), and the fitting curve is also plotted in Fig. 2(b) (dashed curve). For the fitting, we fix $w_0 = 5.9$ μm. The best-fit parameter is $D = 18$ cm^2/s. By using the Einstein relation, the carrier mobility at room temperature is estimated to be $\mu = 710$ cm^2/Vs. Note that the diffusion constant and carrier mobility here do not necessarily correspond to the intrinsic values of this material; that is because the

values estimated from the PL spectra include the effect of photon recycling. If photon recycling occurs, then the diffusion constant can be overestimated [30]. We note that the device performance is determined by the effective mobility including the photon-recycling effect.

For the case of deep excitation, almost no shift of the PL peak is observed, as shown in Fig. 2(c). When d approaches ∞, the second term of Eq. (7) goes to zero. This means that the mean depth should be independent of $w(t)$ when the excitation depth d is sufficiently large. Therefore, the PL peak stays unchanged with time under deep excitation conditions. This behavior can be understood by the following mechanism. The difference of the transmission between d and $d + \Delta d$ can be written as

$$\Delta T = -\alpha e^{-\alpha d} \Delta d. \qquad (10)$$

If d is large, then ΔT goes to zero. In this case, the transmission spectrum hardly changes even though the carrier density profile changes significantly. Therefore, for the case of deep excitation, the PL spectrum does not change even if carrier diffusion occurs and the photocarrier profiles are changed. The fitting parameters for the case of deep excitation with different delay times are summarized in Fig. 2(d). Both δ and σ are almost constant.

In order to obtain a deeper understanding of the photocarrier recombination and diffusion processes, the PL decay curves are shown as a function of the excitation position in Fig. 3(a). The PL decay curves are obtained by spectral integration from 2.0 to 2.6 eV. We find that the PL intensities decrease nonexponentially. One possible explanation for this is related to the carrier diffusion process; more specifically, the PL decay has to be nonexponential if carrier diffusion takes place [11,12]. In our prior work, the PL recombination dynamics have been calculated using a rate equation including carrier diffusion [12]. However, this model is valid only for fast-time ranges of 1 ns. In the long-time regime, the PL decay should slow down due to the
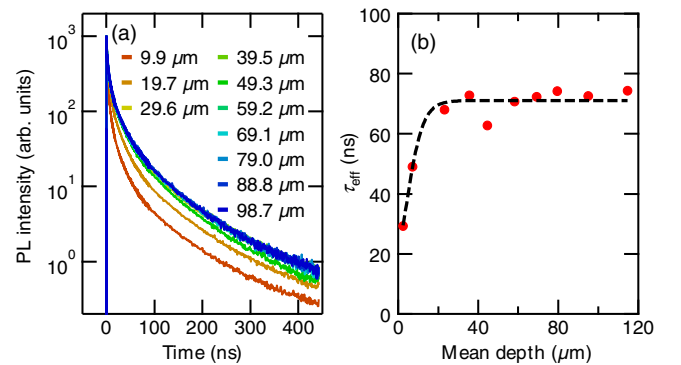
FIG. 3. (a) PL decay curves for different excitation depths. (b) Effective lifetime for different excitation depths. Effective lifetimes are determined from a stretched-exponential function. The dashed line is the fitting curve from Eq. (13).

additional photon-recycling effect, and, thus, the PL dynamics become more complicated. In order to estimate the PL lifetime of the nonexponential decay, we fit the PL decays by a stretched-exponential function,

$$f(t) = A\exp\left[-\left(\frac{t}{\tau}\right)^{\beta}\right]. \qquad (11)$$

Then, we define the effective lifetime τ_{eff} with

$$\tau_{\text{eff}} = \frac{\tau}{\beta}\Gamma\left(\frac{1}{\beta}\right), \qquad (12)$$

where $\Gamma(z)$ is the Γ function. We use the effective lifetime for discussing the excitation-depth dependence of the PL dynamics. The effective lifetimes for different excitation depths are summarized in Fig. 3(b). Here it can be seen that the PL lifetime becomes longer as δ increases. There are two possible mechanisms for this. The first is the enhancement of the emission below the band edge, which is due to photon reabsorption and carrier relaxation. When the excitation depth is large, the photons emitted above the band gap cannot reach the surface because of strong absorption in the sample. Only the lower-energy luminescence can pass through the thick sample. The second reason is the photon recycling. Because of photon reabsorption in combination with high luminescence yields, photocarriers are generated again, and the PL lifetime becomes longer because of the cycles of recombination of the regenerated carriers, luminescence, and reabsorption.

In order to analyze the photon-recycling effect on the PL lifetime, we use a very simple model that takes into account carrier diffusion, recombination, light propagation, and reabsorption. The details of this model are available in the Appendix. According to this model, the PL lifetime including photon recycling can be described as [see Eq. (A8) in the Appendix]

$$\frac{1}{\tau_{\text{eff}}} = \frac{1}{\tau_{\infty}} + \left(\frac{1}{\tau_0} - \frac{1}{\tau_{\infty}}\right)\exp\left(-\frac{\delta}{L_{\text{PR}}}\right). \qquad (13)$$

Here, τ_0 corresponds to the PL lifetime without the photon-recycling effect, and τ_{∞} corresponds to the limit of the PL lifetime in $\delta \to \infty$. L_{PR} is proportional to the carrier diffusion length, the photon propagation length, and the fraction of photons contributing to one cycle of photon recycling [see Eq. (A10) in the Appendix]. In this equation, τ_{eff} approaches τ_0 when δ goes to 0. Using Eq. (13), we are able to analyze the effective-depth dependence of the PL lifetime.

The fitting results obtained using Eq. (13) are plotted as a dashed curve in Fig. 3(b). We obtain the best fit for $\tau_{\infty} = 71$ ns, $\tau_0 = 20$ ns, and $L_{\text{PR}} = 4.2$ μm. The value of τ_{∞} corresponds to the typical value of the PL lifetime

in perovskite thin films [31,32]. We confirm that the PL lifetime without the photon-recycling effect τ_0 is shorter than τ_{∞}. This result shows that the PL lifetime is extended by photon recycling as the effective depth increases. Our calculation suggests that the long PL lifetimes of perovskite thin films are a result of the photon-recycling effect. Previous results of spatially resolved steady-state PL and PC profiles on thin films and devices showed an enhancement of PC intensity and carrier diffusion in solar-cell devices by photon recycling [18]. Our observation of the carrier lifetime is evidence that the effective carrier diffusion is, in fact, enhanced by the photon-recycling effect. The space- and time-resolved spectroscopy reveals that the enhancement of the PL lifetime is an intrinsic bulk effect rather than the extrinsic surface effect in perovskites.

According to our model, the internal luminescence yield Φ_{PL} can be written as follows [see Eq. (A11) in the Appendix]:

$$\Phi_{\text{PL}} = \frac{\tau_{\infty} - \tau_0}{\tau_{\infty} - \eta_{\alpha}\tau_0}, \qquad (14)$$

where η_{α} (=0.54, as shown in the Appendix) is the fraction of reabsorbed photons. We obtain $\Phi_{\text{PL}} = 0.85$. The high value of Φ_{PL} is consistent with previous reports on nanocrystals and films [18,19,33]. Contrary to the high luminescence yields of nanocrystals, low external PL yields have been reported for bulk [34]. The findings in this paper prove that the bulk yield is reduced due to strong reabsorption. The high internal luminescence yield means that perovskite semiconductors have a high potential for optoelectronic devices, such as solar cells, light-emitting diodes, and lasers.

IV. CONCULUSION

In conclusion, we investigate the photocarrier dynamics in $CH_3NH_3PbBr_3$ single crystals using time-resolved two-photon-excitation PL microscopy. We find that the PL spectral shape and PL decay dynamics depend on the depth of the excited and monitored region. As the excitation depth increases, the peak of the PL clearly redshifts, and the lifetime becomes longer. Furthermore, the PL peak redshifts with time when the carriers are excited near the surface. These observations can be well explained by a simple model including photocarrier diffusion and photon-recycling effects. Our data suggest that photon reabsorption plays an important role in the PL dynamics of perovskite materials. According to the findings of this study, it is apparent that lead halide perovskite semiconductors have a huge potential for use in optoelectronic device applications due to high luminescence yields.

APPENDIX PHOTON RECYCLING MODEL

In order to analyze the photon-recycling effect on the PL lifetime, we use a very simple model that takes into account carrier diffusion, recombination, light propagation, and reabsorption. First, we consider the PL lifetime τ_0 for the case without photon recycling. The excited carriers relax by two paths, namely, radiative and nonradiative recombination. Accordingly, the following relation holds:

$$\frac{1}{\tau_0} = \frac{1}{\tau_R} + \frac{1}{\tau_{NR}}. \tag{A1}$$

Here, τ_R and τ_{NR} are the radiative and nonradiative recombination lifetimes, respectively. The internal luminescence yield Φ_{PL} can be written as

$$\Phi_{PL} = \frac{\tau_0}{\tau_R}. \tag{A2}$$

Second, we consider the reabsorption effect. The effective absorption coefficient α_i can be described with

$$\alpha_i = \frac{\int_0^\infty \alpha(E)\gamma_{spon}(E)dE}{\int_0^\infty \gamma_{spon}(E)dE}, \tag{A3}$$

where E, $\alpha(E)$, and $\gamma_{spon}(E)$ are the photon energy, the absorption coefficient, and the spontaneous emission spectrum, respectively. We define the photon propagation length as $L_\alpha = 1/\alpha_i$, which indicates the average distance traveled by emitted photons propagating through the sample. Using Ref. [24], we obtain $L_\alpha = 0.34~\mu m$. The fraction of reabsorbed photons η_α can be written with the following equation:

$$\eta_\alpha = \frac{\int_0^\infty (1 - e^{-\alpha(E)L_\alpha})\gamma_{spon}(E)dE}{\int_0^\infty \gamma_{spon}(E)dE}. \tag{A4}$$

By evaluating this equation, we obtain $\eta_\alpha = 0.54$. One cycle of photon recycling can be imagined as follows. When photon recycling occurs, the excited carriers recombine and emit photons, and the emitted photons are reabsorbed and excite carriers again. Assuming that one electron-hole pair is excited by one photon, the fraction of photons contributing to one cycle of photon recycling η_{PR} can be described as follows:

$$\eta_{PR} = \Phi_{PL}\eta_\alpha. \tag{A5}$$

Third, we estimate the repetition of photon recycling of the carriers excited at the mean depth δ. We suppose that the carriers recombine and emit photons after three-dimensional diffusion with diffusion length L_D given with

$$L_D = \sqrt{6D\tau_0}. \tag{A6}$$

The emitted photons are reabsorbed and excite carriers again after propagating in the sample with the photon propagation length L_α. The repetition of this cycle can be approximated with

$$N_{PR} = \frac{\delta}{\sqrt{L_D^2 + L_\alpha^2}}. \tag{A7}$$

When photon recycling occurs N_{PR} times, the radiative recombination rate is modified according to $1/\tau_R \to (\eta_{PR})^{N_{PR}}/\tau_R$. By way of contrast, the nonradiative recombination rate is modified according to $1/\tau_{NR} \to (1-(\eta_{PR})^{N_{PR}+1})/(1-\eta_{PR})/\tau_{NR}$ because the nonradiative decay path exists in every cycle of photon recycling. At this point, the PL lifetime including photon recycling can be described as

$$\frac{1}{\tau_{eff}} = \frac{1}{\tau_R}(\eta_{PR})^{N_{PR}} + \frac{1}{\tau_{NR}}\frac{1-(\eta_{PR})^{N_{PR}+1}}{1-\eta_{PR}}$$
$$= \frac{1}{\tau_\infty} + \left(\frac{1}{\tau_0} - \frac{1}{\tau_\infty}\right)\exp\left(-\frac{\delta}{L_{PR}}\right), \tag{A8}$$

where

$$\frac{1}{\tau_\infty} = \frac{1}{\tau_{NR}}\frac{1}{1-\eta_{PR}}, \tag{A9}$$

$$L_{PR} = \frac{\sqrt{L_D^2 + L_\alpha^2}}{-\ln(\eta_{PR})}. \tag{A10}$$

Here, τ_∞ corresponds to the lifetime in the limit of $\delta \to \infty$. When δ approaches 0, τ_{eff} goes to τ_0.

According to Eqs. (A1), (A2), (A5), and (A9), Φ_{PL} can be written as follows:

$$\Phi_{PL} = \frac{\tau_\infty - \tau_0}{\tau_\infty - \eta_\alpha\tau_0}. \tag{A11}$$

Now, we can evaluate Φ_{PL} from Eq. (A11).

[1] A. Kojima, K. Teshima, Y. Shirai, and T. Miyasaka, Organometal halide perovskites as visible-light sensitizers for photovoltaic cells, J. Am. Chem. Soc. **131,** 6050 (2009).
[2] NREL Solar efficiency chart, http://www.nrel.gov/pv/assets/images/efficiency_chart.jpg.
[3] S. D. Wolf, J. Holovsky, S.-J. Moon, P. Löper, B. Niesen, M. Ledinsky, F.-J. Haug, J.-H. Yum, and C. Ballif, Organometallic halide perovskites: Sharp optical absorption edge and its relation to photovoltaic performance, J. Phys. Chem. Lett. **5,** 1035 (2014).
[4] Y. Yamada, T. Nakamura, M. Endo, A. Wakamiya, and Y. Kanemitsu, Near-band-edge optical responses of solution-processed organic-inorganic hybrid perovskite

$CH_3NH_3PbI_3$ on mesoporous TiO_2 electrodes, Appl. Phys. Express **7,** 032302 (2014).

[5] S. D. Stranks, V. M. Burlakov, T. Leijtens, J. M. Ball, A. Goriely, and H. J. Snaith, Recombination Kinetics in Organic-Inorganic Perovskites: Excitons, Free Charge, and Subgap States, Phys. Rev. Applied **2,** 034007 (2014).

[6] S. D. Stranks, G. E. Eperon, G. Grancini, C. Menelaou, M. J. P. Alcocer, T. Leijtens, L. M. Herz, A. Petrozza, and H. J. Snaith, Electron-hole diffusion lengths exceeding 1 micrometer in an organometal trihalide perovskite absorber, Science **342,** 341 (2013).

[7] G. Xing, N. Mathews, S. Sun, S. S. Lim, Y. M. Lam, M. Grätzel, S. Mhaisalkar, and T. C. Sum, Long-range balanced electron and hole-transport lengths in organic-inorganic $CH_3NH_3PbI_3$, Science **342,** 344 (2013).

[8] Q. Dong, Y. Fang, Y. Shao, P. Mulligan, J. Qiu, L. Cao, and J. Huang, Electron-hole diffusion lengths >175 μm in solution-grown $CH_3NH_3PbI_3$ single crystals, Science **347,** 967 (2015).

[9] W.-J. Yin, T. Shi, and Y. Yan, Unusual defect physics in $CH_3NH_3PbI_3$ perovskite solar cell absorber, Appl. Phys. Lett. **104,** 063903 (2014).

[10] Y. Yamada, T. Nakamura, M. Endo, A. Wakamiya, and Y. Kanemitsu, Photocarrier recombination dynamics in perovskite $CH_3NH_3PbI_3$ for solar cell applications, J. Am. Chem. Soc. **136,** 11610 (2014).

[11] Y. Yamada, T. Yamada, L. Q. Phuong, N. Maruyama, H Nishimura, A. Wakamiya, Y. Murata, and Y. Kanemitsu, Dynamic optical properties of $CH_3NH_3PbI_3$ single crystals as revealed by one- and two-photon excited photoluminescence measurements, J. Am. Chem. Soc. **137,** 10456 (2015).

[12] T. Yamada, Y. Yamada, H. Nishimura, Y. Nakaike, A. Wakamiya, Y. Murata, and Y. Kanemitsu, Fast free-carrier diffusion in $CH_3NH_3PbBr_3$ single crystals revealed by time-resolved one- and two-photon excitation photoluminescence spectroscopy, Adv. Electron. Mater. **2,** 1500290 (2016).

[13] V. D'Innocenzo, A. R. S. Kandada, M. D. Bastiani, M. Gandini, and A. Petrozza, Tuning the light emission properties by band gap engineering in hybrid lead halide perovskite, J. Am. Chem. Soc. **136,** 17730 (2014).

[14] D. W. de Quiletters, S. M. Vorpahl, S. D. Stranks, H. Nagaoka, G. E. Eperon, M. E. Ziffer, H. J. Snaith, and D. S. Ginger, Impact of microstructure on local carrier lifetime in perovskite solar cells, Science **348,** 683 (2015).

[15] P. Asbeck, Self-absorption effects on the radiative lifetime in GaAs-GaAlAs double heterostructures, J. Appl. Phys. **48,** 820 (1977).

[16] T. Kuriyama, T. Kamiya, and H. Yanai, Effect of photon recycling on diffusion length and internal quantum efficiency in $Al_xGa_{1-x}As$-GaAs heterostructures, Jpn. J. Appl. Phys. **16,** 465 (1977).

[17] P. Renaud, F. Raymond, B. Bensaïd, and C. Vèrié, Influence of photon recycling on lifetime and diffusion coefficient in GaAs, J. Appl. Phys., **71,** 1907 (1992).

[18] L. M. Pazos-Outón, M. Szumilo, R. Lamboll, J. M. Richter, M. Crespo-Quesada, M. Abdi-Jalebi, H. J. Beeson, M. Vrućinić, M. Alsari, H. J. Snaith, B. Ehrler, R. H. Friend, and F. Deschler, Photon recycling in lead iodide perovskite solar cells, Science **351,** 1430 (2016).

[19] S.-T. Ha, C. Shen, J. Zhang, and Q. Xiong, Laser cooling of organic-inorganic lead halide perovskites, Nat. Photonics **10,** 115 (2016).

[20] F. Staub, H. Hempel, J.-C. Hebig, J. Mock, U. W. Paetzold, U. Rau, T. Unold, and T. Kirchartz, Beyond Bulk Lifetimes: Insights into Lead Halide Perovskite Films from Time-Resolved Photoluminescence, Phys. Rev. Applied **6,** 044017 (2016).

[21] O. D. Miller, E. Yablonovitch, and S. R. Kurtz, Strong internal and external luminescence as solar cells approach the Shockley-Queisser limit, IEEE J. Photovoltaics **2,** 303 (2012).

[22] L. Zhu, T. Mochizuki, M. Yoshita, S. Chen, C. Kim, H. Akiyama, and Y. Kanemitsu, Conversion efficiency limits and bandgap designs for multi-junction solar cells with internal radiative efficiencies below unity, Opt. Express **24,** A740 (2016).

[23] M. I. Saidaminov, A. L. Abdelhady, B. Murali, E. Alarousu, V. M. Burlakov, W. Peng, I. Dursun, L. Wang, Y. He, G. Maculan, A. Goriely, T. Wu, O. F. Mohammed, and O. M. Bakr, High-quality bulk hybrid perovskite single crystals within minutes by inverse temperature crystallization, Nat. Commun. **6,** 7586 (2015).

[24] J.-S. Park, S. Choi, Y. Yan, Y. Yang, J. M. Luther, S.-H. Wei, P. Parilla, and K. Zhu, Electronic structure and optical properties of α-$CH_3NH_3PbBr_3$ perovskite single crystal, J. Phys. Chem. Lett. **6,** 4304 (2015).

[25] D. W. de Quilettes, W. Zhang, V. M. Burlakov, D. J. Graham, T. Leijtens, A. Osherov, V. Bulivić, H. J. Snaith, D. S. Ginger, and S. D. Stranks, Photo-induced halide redistribution in organic-inorganic perovskite films, Nat. Commun. **7,** 11683 (2016).

[26] E. T. Hoke, D. J. Slotcavage, E. R. Dohner, A. R. Bowring, H. I. Karunadasa, and M. D. McGehee, Reversible photo-induced trap formation in mixed halide hybrid perovskites for photovoltaics, Chem. Sci. **6,** 613 (2015).

[27] W. van Roosbroeck and W. Shockley, Photon-radiative recombination of electrons and holes in germanium, Phys. Rev. **94,** 1558 (1954).

[28] I. Schnitzer, E. Yablonovitch, C. Caneau, and T. Gmitter, Ultrahigh spontaneous emission quantum efficiency, 99.7% internally and 72% externally, from AlGaAs/GaAs/AlGaAs double heterostructures, Appl. Phys. Lett. **62,** 131 (1993).

[29] M. R. Krames, M. Ochiai-Holcomb, G. E. Höfler, C. Carter-Coman, E. I. Chen, I.-H. Tan, P. Grillot, N. F. Gardner, H. C. Chui, J.-W. Huang, S. A. Stockman, F. A. Kish, M. G. Craford, T. S. Tan, C. P. Kocot, M. Hueschen, J. Posselt, B. Loh, G. Sasser, and D. Collins, High-power truncated-inverted-pyramid $(Al_xGa_{1-x})_{0.5}In_{0.5}P$/GaP light-emitting diodes exhibiting >50% external quantum efficiency, Appl. Phys. Lett. **75,** 2365 (1999).

[30] W. P. Dumke, Spontaneous radiative recombination in semiconductors, Phys. Rev. **105,** 139 (1957).

[31] R. Sheng, A. Ho-Baillie, S. Huang, S. Chen, X. Wen, X. Hao, and M. A. Green, Methylammonium lead bromide perovskite-based solar cells by vapor-assisted deposition, J. Phys. Chem. C **119,** 3545 (2015).

[32] M. Zhang, H. Yu, M. Lyu, Q. Wang, J.-H. Yun, and L. Wang, Composition-dependent photoluminescence intensity and prolonged recombination lifetime of perovskite

$CH_3NH_3PbBr_{3-x}Cl_x$ films, Chem. Commun. (Cambridge) **50**, 11727 (2014).

[33] S. Bhaumik, S. A. Veldhuis, Y. F. Ng, M. Li, S. K. Muduli, T. C. Sum, B. Damodaran, S. Mhaisalkar, and N. Mathews, Highly stable, luminescent core-shell type methylammonium-octylammonium lead bromide layered

perovskite nanoparticles, Chem. Commun. (Cambridge) **52**, 7118 (2016).

[34] S. A. Veldhuis, P. P. Boix, N. Yantara, M. Li, T. C. Sum, N. Mathews, and S. G. Mhaisalkar, Perovskite materials for light-emitting diodes and lasers, Adv. Mater. **28**, 6804 (2016).